HHS Public Access

Author manuscript

Phys Med Biol. Author manuscript; available in PMC 2018 March 07.

Published in final edited form as:

Phys Med Biol. 2017 March 07; 62(5): 1935–1948. doi:10.1088/1361-6560/aa5bc7.

A Monte Carlo study of I-125 prostate brachytherapy with gold nanoparticles: dose enhancement with simultaneous rectal dose sparing via radiation shielding

D. Brivio[1], **P.L. Nguyen**[1], **E. Sajo**[2], **W. Ngwa**[1,2], and **P. Zygmanski**[1]

[1]Brigham & Women's Hospital, Boston, MA, Dana Farber Cancer Institute, Boston, MA, Harvard Medical School

[2]University of Massachusetts Lowell, MA

Abstract

We investigate via Monte Carlo simulations a new ^{125}I brachytherapy treatment technique for High-Risk prostate cancer patients via injection of Au nanoparticle (AuNP) directly into the prostate. The purpose of using the nanoparticles is to increase the therapeutic index via two synergistic effects: enhanced energy deposition within the prostate and simultaneous shielding of organs at risk from radiation escaping from the prostate. Both uniform and non-uniform concentrations of AuNP are studied. The latter are modeled considering the possibility of AuNP diffusion after the injection using brachy needles. We study two extreme cases of coaxial AuNP concentrations: centered on brachy needles and centered half-way between them.

Assuming uniform distribution of 30mg/g of AuNP within the prostate, we obtain a dose enhancement larger than a factor of 2 to the prostate. Non-uniform concentration of AuNP ranging from 10mg/g and 66mg/g were studied. The higher the concentration in a given region of the prostate the greater is the enhancement therein. We obtain the highest dose enhancement when the brachytherapy needles are coincident with AuNP injection needles but, at the same time, the regions in the tail are colder (average dose ratio of 0.7). The best enhancement uniformity is obtained with the seeds in the tail of the AuNP distribution. In both uniform and non-uniform cases the urethra and rectum receive less than 1/3 dose compared to an analog treatment without AuNP.

Remarkably, employing AuNP not only significantly increases dose to the target but also decreases dose to the neighboring rectum and even urethra, which is embedded within the prostate. These are mutually interdependent effects as more enhancement leads to more shielding and vice-versa. Caution must be paid since cold spot or hot spots may be created if the AuNP concentration versus seed position is not properly distributed respect to the seed locations.

Disclosure of conflict of interest

Dr. Brivio, Dr. Sajo, Dr. Ngwa and Dr. Zygmanski have no relevant conflicts of interest to disclose. Dr. Nguyen reports personal fees from Nanobiotix, outside the submitted work and consulted for Medivation, Ferring, and Genome Dx on issues related to prostate cancer, but not directly relevant to this study.

Introduction

According to the American Cancer Society (Anon 2016), prostate cancer is the most common non-skin cancer and the second leading cause of cancer-related death in men in the United States. It is estimated that, in 2016, 180,890 men have been diagnosed with prostate cancer in the United States, and nearly 26,120 men will die of the disease. A recent study showed that on average 21.8% of prostate cancer patients are classified high risk (HR) (Mahmood *et al* 2014). The percentage is much higher at 40.3% for patients over 75 years old. Radiation therapy is a common option (about 36% of cases on average in recent years) to treat prostate cancer especially for those patients with high risk disease (Mahmood *et al* 2014). Noteworthy, HR prostate cancer (Chang *et al* 2014) accounts for nearly all the deaths from prostate cancer. It is known that higher dose to prostate is better for HR patients (Morris *et al* 2015), but increasing dose leads to higher possibility of toxicity, which is an impediment to the patients choosing external beam radio therapy (EBRT) with additional brachytherapy (BT) boost. It has been shown that patients with HR prostate cancer significantly benefit from BT boost added to EBRT (ASCENDE-RT trial (Morris *et al* 2015)). However, both the ASCENDE-RT trial and a similar prior study (Hoskin *et al* 2012) using HDR brachytherapy boost found an increase in the late urethral stricture rate from about 2% to 8%, which gives some clinicians concern about adopting combined modality therapy universally.

With this work we envision the injection of agents made of high-Z nanoparticles such as gold NP (AuNP), hafnium dioxide NP (HfNP), or gadolinium NP (GdNP) directly into prostate and irradiation using brachytherapy seeds. Nanoparticle injection is carried out along tracks parallel to the brachytherapy seed deposition tracks using the same brachytherapy needle template.

These AuNP enhancement agents, when imaged with CT, can be also considered as suitable contrast agents for radiotherapy treatment planning (Hainfeld *et al* 2013). For this reason we will refer to them as contrast/enhancement agents (CEA). With this work we aim to demonstrate that AuNP-based CEA simultaneously increases the dose deposition within the tumor and shields normal organs from the undesired dose. The shielding effect can be conceived as trapping of radiation inside tumor regions filled with agent (trapping of energy decreases the energy leakage outside of the trapping regions). While nanoparticle dose enhancement has been recognized and experimentally demonstrated for various cancer cell types (Butterworth *et al* 2012, Ngwa *et al* 2014), the aforementioned synergistic effect has been neither clearly recognized nor directly utilized in radiotherapy so far. A clinical implementation of high-Z enhancement/shielding agents in radiotherapy may permit effective treatments with more tumor-focused utilization of radiation, and at the same time it may reduce toxicity in healthy tissues and in particular allow EBRT+BT for patients who have already reached the radiotherapy dose limits to normal organ.

Besides the HR group, patients requiring salvage radiation treatment for local recurrence may also benefit from this technique since they may have reached their normal tissue radiotherapy dose limits. Also patients with unfavorable prostate geometry, e.g., particularly long prostates with large contact with rectum who are otherwise suitable candidates for

brachytherapy, may benefit from this proposed treatment because of the greater proximity of the planning target volume (PTV) to a larger area of the rectum. This could be one of several methods to try to reduce the risk of radiation-induced rectal bleeding, enabling this radiotherapy technique also for prostate cancer patients under anticoagulation treatment.

In this theoretical study we investigate the dosimetric benefits and risks of high-Z nanoparticle (NP) based brachytherapy of prostate utilizing radiation ‘sink’ or ‘trap’ effect mentioned above. While these physical effects might have a role to play in other high-Z radiotherapy treatments we study them in a prostate brachytherapy model and we consider injection of nanoparticle agent directly into prostate. Although diffusion of NP agent and its retaining in prostate is not well understood at this time and requires image guided clinical tests to determine the distribution in 3D for specific NP agents, there is an important need to understand dosimetric aspects considering various possible injection tracks and distributions of NP agents. Of particular importance herein is the question of how to plan insertion of catheters with NP agent so that the distribution of NP does not lead to creation of large hot spots or cold spots in the dose distribution. In the case of NP brachytherapy, the effects we focus on may help high risk prostate cancer patients by preferential confinement of radiation within NP laden prostate regions and decreasing urethral and rectal toxicity.

Nanoparticles have the advantage of targeting cancer by being accumulated and entrapped in tumor cells or tumor micro vasculature (Wang and Thanou 2010, Perrault and Chan 2010, Hainfeld *et al* 2013) (active or passive targeting), and have been utilized as contrast agent (CA) for imaging (Wang and Thanou 2010, Perrault and Chan 2010) and vehicles for drugs delivery (Farokhzad and Langer 2009, Kumar *et al* 2015) as well as diagnostic tool for the early detection of precancerous and malignant lesions from biological fluids or biopsied tissue samples (Ferrari 2005, Huo *et al* 2012). Specifically, high-Z NP are known to enhance the nanoscale dose (Tsiamas *et al* 2014a, Ngwa *et al* 2013) delivered by both kilo- and megavoltage x-ray beams owing to the emission of photo-electrons and Auger electrons, which deposit energy in their proximity (at nano-to micrometers distances away from the NP).

Another equally important but less obvious effect is that a region with higher Z tissue (e.g., bone) or contrast/enhancement agent, within lower-Z soft tissue, acts as a radiation “sink” or “trap”. That is, it effectively collects the energy of radiation in the high-Z region and “screens” the lower-Z regions from radiation. This physical effect is due to a complex interplay between Compton and photoelectric interactions followed by Auger or fluorescence emission. The cross-sections of the aforementioned interactions depend on the atomic number (Z), which varies considerably when high-Z enhancement agent is applied, and on the x-ray energy spectrum. It also exhibits a directional dependence at a given energy. The shielding effect of high-Z barriers is well recognized and utilized for radiation protection. Similarly, nanoparticle-induced dose enhancement or radiosensitization has been demonstrated and investigated (Brivio *et al* 2015). However, although the attenuation of flux by tissues with AuNP has already been recognized (Toossi *et al* 2012, Van den Heuvel *et al* 2010), the simultaneous enhancement and trapping of radiation inside the tumor by using high-Z NP is a new concept and application of NP.

So far high-Z NP based radiotherapy has not been clinically used except for few clinical trials. For instance Nanobiotix has recently completed a phase 1 clinical trial with Hafnium oxide NP for soft tissue sarcoma (Bonvalot *et al* 2016) and a phase 2, 3 is starting (Nanobiotix 2016a). Besides that few others phase 1 clinical trials are now open by the same company for other tumors including prostate (Nanobiotix 2016b), liver (Nanobiotix 2015) or head and neck (Nanobiotix 2013). Furthermore, recently the University Hospital in Grenoble (France) has opened a clinical trial with gadolinium based NP for multi-brain metastases (University Hospital Grenoble 2016). High-Z NP based radiation treatment (RT) is still an experimental treatment technique mostly based on theoretical (computational) studies and its efficacy and risks are yet to be determined in the clinical trials.

Our paper points out not only the benefits of AuNP based RT (possibility to enhance dose) but also its risks (possibility to create cold spots). We highlight that these effects are not limited to the case we study in this work (prostate brachytherapy) but they must be carefully considered in all type of high-Z NP based RT. Self-shielding of AuNP agent can be a risk or a benefit depending on how it is used in the treatment planning and delivery of treatment. We show that if properly utilized the shielding effect can be a benefit in shielding the organs at risk (OAR) from the undesired radiation. However, if not properly used, it can lead to creation of cold spots in the tumor regions. Efficient utilization of AuNP enhancement and shielding effects requires treatment plan optimization. Our results lead us to conclude that an optimized (most likely inverse) treatment planning approach is required to obtain more uniform (across the whole prostate) dose enhancement without extreme hot spots or cold spots. However, because not all concentrations of AuNP agent are feasible in practice, optimization must be based on imaging and involve seed placement as well.

Materials and Method

To demonstrate these effects and their suitability for high-risk cancer treatment, we performed Monte Carlo simulations in 3D anatomical phantoms using ^{125}I brachytherapy seeds.

Uniform (30mg/g) and heterogeneous (ranging from 10 mg/g to 66 mg/g) macroscopic concentration distributions of AuNP contrast agent were studied. It should be noted that at present there are no experimental data about the actual concentrations of AuNP agent achievable by direct injection into prostate. Concentration values of 37.5mg/g were obtained via direct injection into eye (Kang *et al* 2009), and of 50mg/ml into mice tumor tissues (Hainfeld *et al* 2014). Bonvalot et al. reported the direct NP injection of 53.3g/L in human soft tissue sarcoma of the limbs (Bonvalot *et al* 2016). The total mass of injected AuNP (about 2 g) was kept the same for both uniform and non-uniform distributions. The former is an idealistic scenario, in which the contrast agent is homogenized across the whole PTV volume (Fig. 1a). While this is not fully feasible, it gives a limiting condition as a reference for more realistic distributions of the AuNP contrast. The heterogeneous distributions account for two extreme scenarios: when the concentration of the contrast agent is highest along the insertion track of the brachy needle, and when it is highest in between the needle tracks (Fig 1b and c). The approach in Fig. 1c will require about twice as many needle insertions. As it will be shown, the resulting dose distribution inside PTV and OARs

significantly differ depending on the loading type of the contrast with respect to seed loading.

Coupled photon-electron Monte Carlo simulations were performed using the MCNP6 computer code (Goorley *et al* 2012) with photon and electron cut off energy of 1keV. Full photon-induced relaxation cascade was considered with the atomic relaxation data were taken from the *eprdata12* library.

The simulation geometry for the ^{125}I seed was developed based on the Oncura™ Model 6711 (manufactured by GE Healthcare, IL, marketed by Oncura, Inc.), according to the details reported by Dolan (Dolan *et al* 2006) and following the directions of the TG-43U1 protocol (Rivard *et al* 2004). The seed consisted of an Ag rod coated with radioactive material and encapsulated in a Ti shell (see Fig. 2a). The radioactive layer (2 μm thick) consisted of a silver halide mixture of AgBr and AgI present in a 2.5:1 molecular ratio (Dolan *et al* 2006). ^{125}I spectrum reported in TG-43U1 (Rivard *et al* 2004) was considered. The Ti shell also included air with 40% humidity; air composition was taken from table XIV in TG-43U1 (Rivard *et al* 2004). Additional details of the model are shown in Fig. 2a.

Dose distributions in terms of radial dose function and 2D anisotropy function were studied by placing a single seed at the center of a spherical water phantom (30cm diameter) and scoring the F6 tally (dose in charged particle equilibrium) in toroidal voxels with 0.2 mm radius about the cylindrically symmetric seed, and in spherical voxels with 0.5 mm radius along the seed axis. 5.0×10^7 histories were used giving a relative MC error of lower than 3% for tori at different angles and radii, and lower than 5% for the spheres along the seed axis.

Using the seed geometry detailed above we also simulated brachytherapy seed implants in an anatomical model of the prostate (ellipsoid, 63.6 cm^3) using uniform and non-uniform AuNP concentrations. Urethra (cylinder, diameter 5 mm) and rectum (cylinder, external radius 0.85 cm, wall thickness 0.4 cm) did not contain the enhancement agent. We simulated the brachytherapy treatment by placing 74 ^{125}I seeds uniformly throughout the entire prostate except in the urethra. As shown in Fig. 1a 24 ^{125}I seed needles are inserted parallel to the rectum. Needles are spaced 0.85 cm apart and the seeds along each needle are 1 cm apart. Alternating loading of seeds in neighboring needles was implemented to obtain a uniform dose distribution. Notice the lack of the central needle to spare urethra. Each seed used in the multi-source simulation was compared to the original one in terms of emission spectra and emitting positions inside the seed geometry and they were found identical. AuNP-filled tissue was modeled as composed of water and gold such that the Au concentration in water was calculated as $c=\frac{m_{Au}}{m_{tot}}$. This study aimed to show the effect of uniform and non-uniform distributions of AuNP in the whole prostate volume during a brachytherapy treatment (AuNP-BT) versus standard brachytherapy treatment (STD BT) without gold nanoparticles. We performed three different simulations:

- **a.** a) uniform concentration of 30 mg/g in the entire prostate (Fig. 1a);
- **b.** b) non-uniform concentration with the position of brachytherapy needles coincident with AuNP injection needles;

c. c) non-uniform concentration with AuNP needles in intermediate positions with respect to the brachy needles.

The distribution of AuNP agent in cases b) and c) are limited by the insertion path of the needles with AuNP agent and its diffusion away from the point of injection. Non-uniform distributions were simulated by dividing a total of 1.96 g AuNP mass into three regions around the axis of an injection needle (see Fig. 1b and 1c): *Center* with high concentration (obtained from the intersection of cylinders of 2mm radius with the prostate ellipsoid), *Gradient* with intermediate concentration (intersection of two cylinders with 2 mm and 4 mm radii with prostate ellipsoid) and *Tail* region filling the rest of the prostate with lower AuNP concentration. In case b) ^{125}I seeds were placed in the region with highest AuNP concentration, while in case c) the seeds were located in the *tail* of AuNP distribution. The concentration of AuNP in the three regions were calculated with the assumptions c_{Tail}=10 mg/g and $c_{Center}=2c_{Gradient}$. In this way, the concentrations in case b) c_{Center}=66mg/g, $c_{Gradient}$=33mg/g, c_{Tail}=10mg/g; and in case c) c_{Center}=64.6mg/g, $c_{Gradient}$=32.3mg/g, c_{Tail}=10mg/g. The simulations were run for 10^8 histories and dose was computed scoring F6 (kerma) and *F8 (total energy deposited by photons and electrons with proper division by mass) tallies in the regions of interest. Because F6 assumes charged particle equilibrium, the difference between the two tallies was up to 1% in the AuNP filled volume. The mesh tally RMESH3 (which is based on F6 tally) was used for obtaining 3D dose distribution using 0.2 × 0.2 × 0.2 cm^3 voxels in the prostate and rectum wall, and 0.1 × 0.1 × 0.2 cm^3 voxels in the urethra. The relative error per voxel (obtained from RMESH3 statistical uncertainties) was lower than 2.5% in the prostate and lower than 5% in rectum and urethra.

Results

Single seed dosimetric study

As shown in Fig. 2, the dose distribution of a single ^{125}I seed placed at the center of a 30cm diameter water phantom was found in general agreement with experimental and MC data available in literature (Rivard *et al* 2004, Dolan *et al* 2006, Williamson 1991, Kennedy *et al* 2010). In particular, the radial dose function normalized using a linear-source geometry function $g_L(r)$ and the 2D anisotropy function $F(r,\theta)$ are in good agreement with the consensus data approved by TG-43U1 protocol (Rivard *et al* 2004). For instance the maximum percentage difference between this work and TG-43U1 consensus data in the radial dose function $g_L(r)$ and in the 2D anisotropy function are respectively 0.9% and 3%. Definition of these two distribution functions can be found in TG-43U1 (Rivard *et al* 2004). Model 6711 of the ^{125}I source was used in all the simulation reported in this paper.

Multiple seeds

Fig. 3 compares the total dose per simulation history in the different regions of the prostate, plus the urethra and the rectum for the three simulation geometries. Compared to standard treatment, in the presence of uniform AuNP distribution the total dose in the whole prostate volume is increased by a factor of 2.3 (Fig. 3a), while the total dose in the rectum and urethra is reduced to about 1/3 of the standard dose. Placing the seeds in the *Center* region with higher AuNP concentration (case b) produces the highest dose enhancement

(DER=5.4) in that portion of the prostate and an appreciable enhancement in the *Gradient* region (DER=1.8) but prevents part of the radiation from reaching the *Tail* region (DER=0.7). In contrast, placing the seed in the *Tail* of the AuNP concentration produces a significant enhancement in the whole prostate (DER of 3.1, 2.4 and 1.4 respectively for *Center*, *Gradient* and *Tail*). All of the simulations with AuNP (both uniform and non-uniform) show substantial urethra and rectum sparing, as they receive about 1/3 of the standard dose. These results highlight the benefits of AuNP-BT combined treatment and also the need for the development of treatment planning methods using AuNP and BT seeds to improve dose uniformity within the prostate.

Fig. 4 displays the cumulative dose volume histograms (DVH) for prostate, urethra and rectum wall, which are shown for the case when the prostate is loaded with Au nanoparticles (solid lines) versus without AuNP (dashed lines). Cases a), b) and c) correspond to different AuNP concentrations, as described above, and shown in Fig. 1. The total delivered dose was calculated as the integral over the entire lifetime of ^{125}I using seeds having air kerma strength of 1.467 U each. ^{125}I source strength was chosen to give a BT boost to EBRT. The increased dose to the prostate and decreased dose to the urethra and the rectum relative to the standard treatment are indicated with right and left arrows, respectively. Case b) corresponds to non-uniform concentration with seeds in the *Center* region. It is noticeable that a portion of the prostate receives lower dose compared to the standard treatment (*Tail* region as also shown in Figure 3b). Fig 4c indicates that this portion (small corner of the dashed blue line above the solid blue line at about 110 Gy) can be substantially reduced using a different positioning of the AuNP needles and brachy catheters. The optimization of the positioning requires dedicated treatment planning and it is beyond the scope of this work.

In Table 1 we report D90, V100, V150, V200, V250, V300 for prostate and V100, D30, D10 for urethra and rectum under the different scenarios. D90 is defined as the minimum dose covering 90% of the prostate volume. V100, V150, V200, V250, V300 are defined as the percentage volume of the prostate receiving at least 100%, 150%, 200%, 250% and 300% of the prescribed minimal peripheral dose (mPD), respectively. D30 and D10 are defined as the minimum dose covering 30% and 10% of the urethra or the Rectum walls. We set mPD to 110Gy in the STD BT treatment. In parenthesis the ratio respect to the STD BT treatment.

To visualize some of these comments and arguments we present in Figure 5 the simulation results of dose distribution at the axial, sagittal and coronal planes intersecting at the center of the prostate for the STD BT and the aforementioned three AuNP-BT scenarios. Seed positions in the plane of the central slice are in the areas of the red/white hot spots. In the treatment with uniform distribution of AuNP (case a), the hot spots are in the same position but hotter and the rest of the prostate receives higher dose as well and dose outside of prostate is reduced. In the treatment with non-uniform distributions of AuNP (case b and c) the hot spots positions are similar to the uniform case a) but the dose distribution is changed, and the dose outside is strongly reduced as well. Note the dose coverage of the prostate changes for the three AuNP-BT cases if the distribution, number and strength of the seed are the same for all three of them. This can be adjusted by customizing the seeds strengths or their number and distribution for each treatment case.

The best AuNP distribution from the three studied is the uniform one, but it is not realistic. However the distribution with AuNP interspaced with seeds is more representative of what might be achievable in practice. In this scenario (case c)) interspaced distribution aims to enhance more the tails and less the peaks of the standard dose distribution around the seeds. The result is close to that for uniform concentration both in term of isodose distribution and of DVH. It does not show the cold spots of the case with AuNP centered on the seeds. The counterpart is that such injection would require about twice as many needles insertion in the prostate.

Discussion and conclusions

In this work we studied AuNP radiation effects in prostate ^{125}I LDR brachytherapy model. In particular, we showed the importance of radiation sink or trapping effect that leads to shielding not only of external to PTV organs at risk (rectum) but also internal (urethra). We demonstrated via Monte Carlo simulation that a synergistic effect of dose enhancement and radiation trapping can be achieved both for uniform and nonuniform distributions of high-Z nanoparticle contrast agent.

The radiation-trapping phenomenon occurs because high-Z NP absorb x-ray radiation and emit many low-energy electrons, which are absorbed in the tissue within nano- to micrometers away from the nanoparticles. The overall effect of their presence is a containment of radiation to the cancer cells surrounding the nanoparticle and significant reduction of stray radiation outside of the tumor. In the standard radiotherapy treatment the photons are only partially stopped by the tumor and therefore they deposit a relatively large amount of their energy outside of it. In the proposed technique the injected agent acts as a trap of radiation effectively shielding the organs at risk (rectum and urethra) from the undesired dose. As we have shown above a non-uniform NP distribution and certain positioning of radioactive seed may prevent radiation from reaching some prostate regions located behind a volume with high NP concentration (loss of local control).

Macroscopic regions with containing nanoparticle agents enhance energy deposition both at macroscopic (tissue/organ) and nanoscopic (cellular) levels (Zygmanski and Sajo 2016, McMahon *et al* 2011). A full detailed analysis of the dose distribution around AuNP would require nanoscopic voxels and knowledge of location of nanoparticles or nanoparticle clusters with respect to cellular targets (cancer cells or cancer microvasculature.) but only few microscopic regions of interest can be evaluated in this way. Fortunately, it has been shown (Tsiamas *et al* 2013, 2014b) that while the dose enhancement averaged over macroscopic voxels is much smaller than the dose enhancement on the surface of AuNPs, it is a useful metric of overall properties of enhancement when various spectra or regions of body or irradiation techniques are compared to each other. In the present work we addressed only the macroscopic effects in mm-size voxels. The macroscopic dose enhancement or dose reduction effects are equally important as nanoscopic effects for safe and proper utilization of AuNP agents, irrespective if they are injected via bloodstream or directly into the tumor.

Results show that while dose enhancement to the prostate and sparing of organs at risk are possible, caution must be exercised whenever realistic AuNP distributions are employed

since the relative position of the radioactive seeds and the high-concentration AuNP region may be suboptimal, leading to underdosing some prostate areas, if high-Z NP distribution is not carefully planned and controlled. Thus the best strategy to fully exploit the benefits of high-Z contrast enhanced brachytherapy is to perform optimized treatment planning based on CT data with and without nanoparticle agent.

Experimentally, only quasi-uniform distributions or non-uniform distributions are feasible and NP diffusion time may play an important role. Therefore, parallel experimental investigations about the best NP size, uniformity and long term stability of AuNP uptake versus leakage are required. Depending on the stability over time, the appropriate irradiation technique can be developed, including the selection of brachytherapy seed type (^{125}I has 59.4 days half life, ^{103}Pd has 16.991 days half life with similar photon energies as ^{125}I) or the use external beam, to obtain optimal results. A further possibility is the use high dose rate (HDR) brachytherapy employing ^{192}Ir with remote afterloading technique. However, the higher energy and therefore larger penetration depth of ^{192}Ir makes it less favorable than ^{125}I or ^{103}Pd.

From another perspective, HDR BT with high-Z NP would also have an immediate application to other cancers such gynecologic cancer. As mentioned, this technique may employ NP made of any materials with high atomic number. Alternatives to AuNP are gadolinium NP (Sancey *et al* 2014) or hafnium oxide NP (Marill *et al* 2014). The latter are already FDA approved and are currently employed for a phase II/III clinical trial with patients with soft tissue sarcoma (Nanobiotix 2016a) while GdNP will soon start a clinical trial on multi-brain metastases in France (Kotb *et al* 2016). A multicenter clinical trial is being launched recently in prostate cancer (Nanobiotix 2016b).

High-risk (HR) prostate cancer patients may benefit from this AuNP BT combined technique since they often require a radiation boost. HR prostate patients constitute a large part of the total population of prostate cancer patients and account for almost all deaths. Besides high risk patients, three other categories of patients may directly benefit: patients (a) requiring salvage radiation treatment for local recurrence, (b) those with unfavorable prostate geometry and (c) those under anticoagulation treatment. High-Z nanoparticle based treatment may offer substantial benefits to all prostate cancer patients receiving brachytherapy and external radiotherapy treatments. The use of high-Z nanoparticles prostate radiotherapy may result in lower toxicity to normal healthy tissue (rectum and urethra) and higher tumor cell dose boost. It should be noted that direct urethral involvement of tumor has been reported in 2%–7% of cases (Huang *et al* 2007, Padilha *et al* 2013), and our urethral-sparing technique may be suboptimal for these patients. Therefore, this technique may be best used on patients whose endorectal coil MRIs do not show disease approaching the urethra.

Boosting only the intra-prostatic lesion (IPL) is potentially attractive in that it can target the highest concentration of visible tumor without significantly enhancing toxicity, but this strategy remains unproven particularly for patients with higher-risk disease. Thus far, all of the trials that have demonstrated a benefit to dose escalation in prostate cancer have treated the entire gland to the higher dose. One major reason for this is the inherent multifocal

nature of prostate cancer in which the most dangerous lesion (i.e. highest grade lesion) is not necessarily the largest or dominant lesion. If one would wish to boost ILP only since the dose fall off is sharper at the edges of AuNP distribution we would suggest to inject NP inside the IPL and outside with few mm extra margin respect to a standard treatment isodose (1–2mm).

Because this technique creates sharper dose gradients at the prostatic capsule, it would be best to limit it to patients who do not have any evidence of extracapsular disease on MRI, particularly 3T multiparametric MRI with endorectal coil, which offers excellent specificity, and reasonable (but not perfect) sensitivity for extracapsular extension (Otto *et al* 2014).

It should be noted also that with nanoparticle enhancement cold-spots may be amplified as well (i.e. become colder), and so it is critical to pay attention to good seed implant and NP agent injection techniques when using nanoparticles.

Finally, experimental studies on the AuNP distributions and the feasibility in animal models need to be demonstrated before this technique may become clinically available. Beside the application of the presented technique to the particular prostate case, dose enhancement vs shielding or trapping of radiation must be carefully addressed in all clinical implementation of high-Z NP for radiation treatments.

Acknowledgments

This work was supported by JCRT grant and by NIH National Cancer Institute grant 1 K01 CA172478-01. We are grateful to R. Cormack and M. Makrigiorgos for constructive suggestions and support.

References

Anon. American Cancer Society. 2016. http://www.cancer.org/cancer/prostatecancer/ Online: http://www.cancer.org/cancer/prostatecancer/

Bonvalot S, Le Pechoux C, Debaere T, Kantor G, Buy X, Stoeckle E, Sargos P, Terrier P, Coindre JJ-m, Lassau N, AIT SARKOUH R. Dimitriu M, Borghi E, Levy L, Deutsch E, Soria JC. First Human Study Testing a New Radio Enhancer Using Nanoparticles (NBTXR3) Activated by Radiation Therapy in Patients with Locally Advanced Soft Tissue Sarcomas. Clin Cancer Res. 2016 Oct 6, 2016.

Brivio D, Zygmanski P, Arnoldussen M, Hanlon J, Chell E, Sajo E, Makrigiorgos GM, Ngwa W. Kilovoltage radiosurgery with gold nanoparticles for neovascular age-related macular degeneration (AMD): a Monte Carlo evaluation. Phys Med Biol. 2015; 60:9203–13. [PubMed: 26576672]

Butterworth KT, McMahon SJ, Currell FJ, Prise KM. Physical basis and biological mechanisms of gold nanoparticle radiosensitization. Nanoscale. 2012; 4:4830. [PubMed: 22767423]

Chang AJ, Autio KA, Roach M, Scher HI. High-risk prostate cancer-classification and therapy. Nat Rev Clin Oncol. 2014; 11:308–23. [PubMed: 24840073]

Dolan J, Lia Z, Williamson JF. Monte Carlo and experimental dosimetry of an I 125 brachytherapy seed. Med Phys. 2006; 33:4675–84. [PubMed: 17278820]

Farokhzad OC, Langer R. Impact of nanotechnology on drug delivery. ACS Nano. 2009; 3:16–20. [PubMed: 19206243]

Ferrari M. Cancer nanotechnology: opportunities and challenges. Nat Rev Cancer. 2005; 5:161–71. [PubMed: 15738981]

Goorley T, James M, Booth T, Brown F, Bull J, Cox L, Durkee J, Elson J, Fensin M, Forster R, Hendricks J, Hughes H, Johns R, Kiedrowski B, Martz R, Mashnik S, Mckinney G, Pelowitz D,

Prael R, Sweezy J, Waters L, Wilcox T, Zukaitis T. Initial MCNP6 Release Overview. Nucl Technol. 2012; 180:298–315.

Hainfeld JF, Lin L, Slatkin DN, Avraham Dilmanian F, Vadas TM, Smilowitz HM. Gold nanoparticle hyperthermia reduces radiotherapy dose. Nanomedicine Nanotechnology, Biol Med. 2014; 10:1609–17.

Hainfeld JF, Smilowitz HM, O'Connor MJ, Dilmanian FA, Slatkin D. Gold nanoparticle imaging and radiotherapy of brain tumors in mice. Nanomedicine (Lond). 2013; 8:1601–9. [PubMed: 23265347]

Van den Heuvel F, Locquet J-P, Nuyts S. Beam energy considerations for gold nano-particle enhanced radiation treatment. Phys Med Biol. 2010; 55:4509–20. [PubMed: 20668345]

Hoskin PJ, Rojas AM, Bownes PJ, Lowe GJ, Ostler PJ, Bryant L. Randomised trial of external beam radiotherapy alone or combined with high-dose-rate brachytherapy boost for localised prostate cancer. Radiother Oncol. 2012; 103:217–22. [PubMed: 22341794]

Huang WC, Kuroiwa K, Serio AM, Bianco FJ, Fine SW, Shayegan B, Scardino PT, Eastham JA. The Anatomical and Pathological Characteristics of Irradiated Prostate Cancers May Influence the Oncological Efficacy of Salvage Ablative Therapies. J Urol. 2007; 177:1324–9. [PubMed: 17382724]

Huo Q, Litherland SA, Sullivan S, Hallquist H, Decker DA, Rivera-Ramirez I. Developing a nanoparticle test for prostate cancer scoring. J Transl Med. 2012; 10:44. [PubMed: 22404986]

Kang SJ, Durairaj C, Kompella UB, O'Brien JM, Grossniklaus HE. Subconjunctival nanoparticle carboplatin in the treatment of murine retinoblastoma. Arch Ophthalmol. 2009; 127:1043–7. [PubMed: 19667343]

Kennedy RM, Davis SD, Micka JA, DeWerd LA. Experimental and Monte Carlo determination of the TG-43 dosimetric parameters for the model 9011 THINSeed brachytherapy source. Med Phys. 2010; 37:1681–8. [PubMed: 20443489]

Kotb S, Detappe A, Lux F, Appaix F, Barbier EL, Tran V-L, Plissonneau M, Gehan H, Lefranc F, Rodriguez-Lafrasse C, Verry C, Berbeco R, Tillement O, Sancey L. Gadolinium-Based Nanoparticles and Radiation Therapy for Multiple Brain Melanoma Metastases: Proof of Concept before Phase I Trial. Theranostics. 2016; 6:418–27. [PubMed: 26909115]

Kumar R, Belz J, Markovic S, Jadhav T, Fowle W, Niedre M, Cormack R, Makrigiorgos MG, Sridhar S. Nanoparticle-based brachytherapy spacers for delivery of localized combined chemoradiation therapy. Int J Radiat Oncol Biol Phys. 2015; 91:393–400. [PubMed: 25636762]

Mahmood U, Levy LB, Nguyen PL, Lee AK, Kuban DA, Hoffman KE. Current Clinical Presentation and Treatment of Localized Prostate Cancer in the United States. J Urol. 2014; 192:1650–6. [PubMed: 24931803]

Marill J, Anesary NM, Zhang P, Vivet S, Borghi E, Levy L, Pottier A. Hafnium oxide nanoparticles: toward an in vitro predictive biological effect? Radiat Oncol. 2014; 9:1–11. [PubMed: 24382205]

McMahon SJ, Hyland WB, Muir MF, Coulter JA, Jain S, Butterworth KT, Schettino G, Dickson GR, Hounsell AR, O'Sullivan JM, Prise KM, Hirst DG, Currell FJ. Biological consequences of nanoscale energy deposition near irradiated heavy atom nanoparticles. Sci Rep. 2011; 1:18. [PubMed: 22355537]

Morris WJ, Tyldesley S, Pai HH, Halperin R, McKenzie MR, Duncan G, Morton G, Murray N, Hamm J. ASCENDE-RT*: A multicenter, randomized trial of dose-escalated external beam radiation therapy (EBRT-B) versus low-dose-rate brachytherapy (LDR-B) for men with unfavorable-risk localized prostate cancer. J Clin Oncol. 2015; 33

Nanobiotix. NBTXR3 Crystalline Nanoparticles and Radiation Therapy in Treating and Randomized Patients in Two Arms With Soft Tissue Sarcoma of the Extremity and Trunk Wall. Bethesda Natl Libr Med (US) 2007. 2016a. Available from https//clinicaltrials.gov/ct2/show/NCT02379845 NLM identifier NCT02379845 Online: https://clinicaltrials.gov/ct2/show/NCT02379845

Nanobiotix. NBTXR3 Crystalline Nanoparticles and Radiation Therapy in Treating Patients With Locally Advanced Squamous Cell Carcinoma of the Oral Cavity or Oropharynx. Bethesda Natl Libr Med (US) 2007. 2013. Available from https//clinicaltrials.gov/ct2/show/NCT01946867 NLM identifier NCT01946867 Online: https://clinicaltrials.gov/ct2/show/NCT01946867

Nanobiotix. NBTXR3 Crystalline Nanoparticles and Stereotactic Body Radiation Therapy in the Treatment of Liver Cancers. Bethesda Natl Libr Med (US) 2007. 2015. Available from https://clinicaltrials.gov/ct2/show/NCT02721056 NLM identifier NCT02721056 Online: (https://clinicaltrials.gov/ct2/show/NCT02721056

Nanobiotix. NBTXR3 Nanoparticles and EBRT or EBRT With Brachytherapy in the Treatment of Prostate Adenocarcinoma. Bethesda Natl Libr Med (US) 2007. 2016b. Available from https://clinicaltrials.gov/show/NCT02805894 NLM identifier NCT02805894 Online: https://clinicaltrials.gov/show/NCT02805894

Ngwa W, Korideck H, Kassis AI, Kumar R, Sridhar S, Makrigiorgos GM, Cormack RA. In vitro radiosensitization by gold nanoparticles during continuous low-dose-rate gamma irradiation with I-125 brachytherapy seeds. Nanomedicine. 2013; 9:25–7. [PubMed: 23041410]

Ngwa W, Kumar R, Sridhar S, Korideck H, Zygmanski P, Cormack RA, Berbeco R, Makrigiorgos GM. Targeted radiotherapy with gold nanoparticles: current status and future perspectives. Nanomedicine (Lond). 2014; 9:1063–82. [PubMed: 24978464]

Otto J, Thörmer G, Seiwerts M, Fuchs J, Garnov N, Franz T, Horn L C, Do MH, Stolzenburg JU, Kahn T, Moche M, Busse H. Value of endorectal magnetic resonance imaging at 3T for the local staging of prostate cancer *RoFo Fortschritte auf dem Gebiet der Rontgenstrahlen und der Bildgeb*. Verfahren. 2014; 186:795–802.

Padilha MM, Stephen Jones J, Streator Smith K, Zhou M, Walker E, Magi-Galluzzi C. Prediction of prostate cancer to urethra distance by a pretreatment nomogram: urethral thermoprotection implication in cryoablation. Prostate Cancer Prostatic Dis. 2013; 16:372–5. [PubMed: 23999668]

Perrault SD, Chan WCW. In vivo assembly of nanoparticle components to improve targeted cancer imaging. Proc Natl Acad Sci U S A. 2010; 107:11194–9. [PubMed: 20534561]

Rivard MJ, Coursey BM, DeWerd LA, Hanson WF, Huq MS, Ibbott GS, Mitch MG, Nath R, Williamson JF. Update of AAPM Task Group No. 43 Report: A revised AAPM protocol for brachytherapy dose calculations. Med Phys. 2004; 31:633–74. [PubMed: 15070264]

Sancey L, Lux F, Kotb S, Roux S, Dufort S, Bianchi A, Crémillieux Y, Fries P, Coll J-L, Rodriguez-Lafrasse C, Janier M, Dutreix M, Barberi-Heyob M, Boschetti F, Denat F, Louis C, Porcel E, Lacombe S, Le Duc G, Deutsch E, Perfettini J-L, Detappe A, Verry C, Berbeco R, Butterworth KT, McMahon SJ, Prise KM, Perriat P, Tillement O. The use of theranostic gadolinium-based nanoprobes to improve radiotherapy efficacy. Br J Radiol. 2014; 87:20140134. [PubMed: 24990037]

Toossi MTB, Ghorbani M, Mehrpouyan M, Akbari F, Sabet LS, Meigooni AS. A Monte Carlo study on tissue dose enhancement in brachytherapy: A comparison between gadolinium and gold nanoparticles. Australas Phys Eng Sci Med. 2012; 35:177–85. [PubMed: 22700179]

Tsiamas P, Liu B, Cifter F, Ngwa WF, Berbeco RI, Kappas C, Theodorou K, Marcus K, Makrigiorgos MG, Sajo E, Zygmanski P. Impact of beam quality on megavoltage radiotherapy treatment techniques utilizing gold nanoparticles for dose enhancement. Phys Med Biol. 2013; 58:451–64. [PubMed: 23302438]

Tsiamas P, Mishra P, Cifter F, Berbeco RI, Marcus K, Sajo E, Zygmanski P. Low-Z linac targets for low-MV gold nanoparticle radiation therapy. Med Phys. 2014a; 41:21701.

Tsiamas P, Sajo E, Cifter F, Theodorou K, Kappas C, Makrigiorgos M, Marcus K, Zygmanski P. Beam quality and dose perturbation of 6MV flattening-filter-free linac. Phys Medica. 2014b; 30:47–56.

University Hospital Grenoble. Radiosensitization of Multiple Brain Metastases Using AGuIX Gadolinium Based Nanoparticles (NANO-RAD). Bethesda Natl Libr Med (US) 2007. 2016. Available from https//clinicaltrials.gov/ct2/show/NCT02820454 NLM identifier NCT02820454 Online: https://clinicaltrials.gov/ct2/show/NCT02820454

Wang M, Thanou M. Targeting nanoparticles to cancer. Pharmacol Res. 2010; 62:90–9. [PubMed: 20380880]

Williamson JF. Comparison of measured and calculated dose rates in water near I-125 and Ir-192 seeds. Med Phys. 1991; 18

Zygmanski P, Sajo E. Nanoscale radiation transport and clinical beam modeling for gold nanoparticle dose enhanced radiotherapy (GNPT) using X-rays. Br J Radiol. 2016; 89:20150200. [PubMed: 26642305]

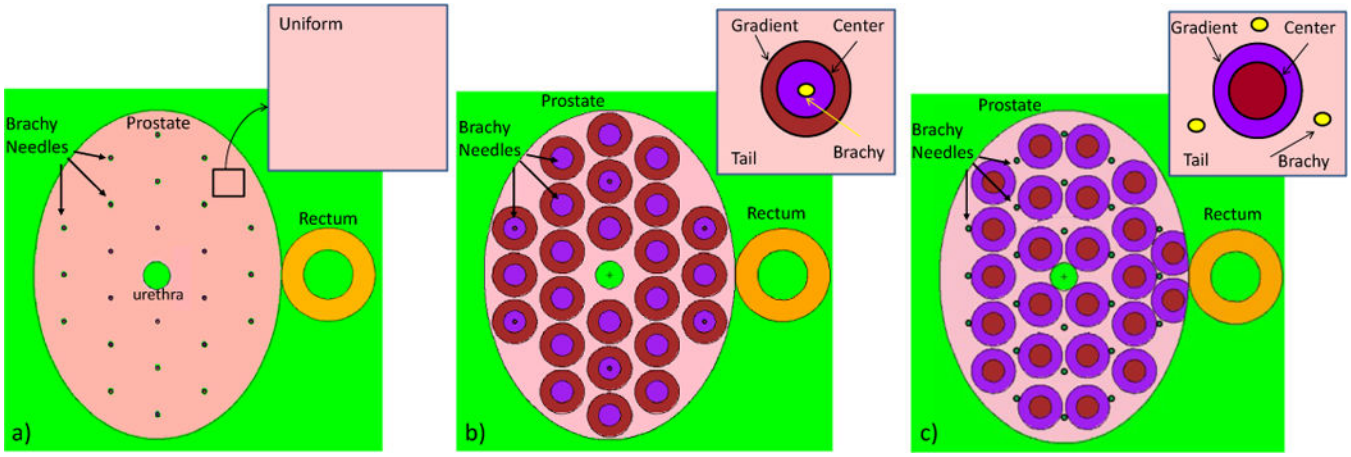

Figure 1.

Treatment geometries: a) with uniform AuNP concentration (30 mg/g) in the entire prostate volume; b) and c) with non-uniform AuNP concentration, which is divided into three regions: Center, Gradient (intersection of cylinders with prostate ellipsoid) and Tail region filling the rest of the prostate. b) Brachytherapy needles (and ^{125}I seeds) are centered in the region with higher AuNP concentration (Center region). c) ^{125}I seeds are in the Tail of the AuNP concentration. In all the geometries a), b) and c) the total mass of Au is constant at 1.96 g. Concentration in b) and c) are calculated assuming c_{Tail}=10mg/g and c_{Center}=2 $c_{Gradient}$, therefore concentration values are as follows: b) c_{Center}=66mg/g, $c_{Gradient}$=33mg/g, c_{Tail}=10mg/g; c) c_{Center}=64.6mg/g, $c_{Gradient}$=32.3mg/g, c_{Tail}=10mg/g.

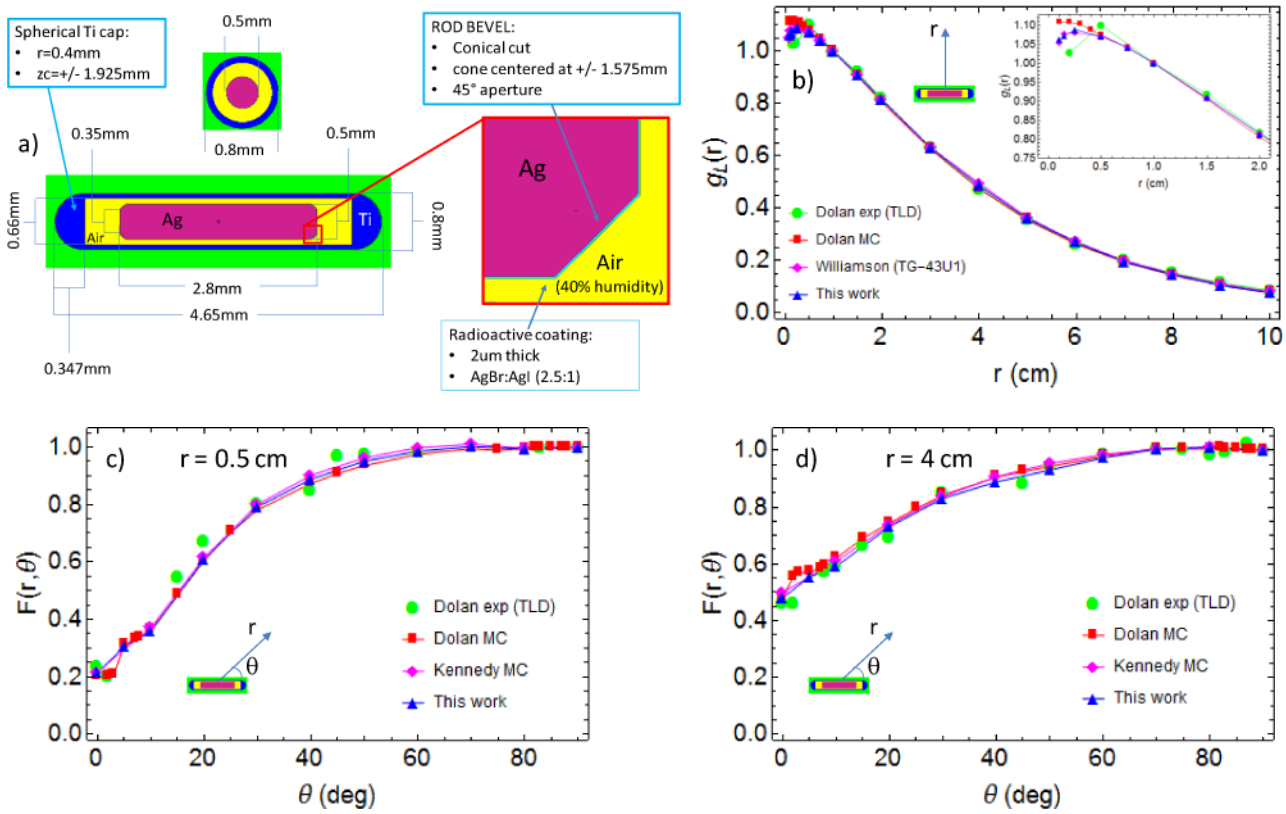

Figure 2.

(a) ^{125}I seed Model 6711 MCNP geometry details; (b) radial dose function with line-source geometry function normalization $g_L(r)$ (see Eqs. (4) and (6) in TG-43U1 (Rivard et al 2004)), Williamson (Williamson 1991) refer to TG-43U1 consensus MC data; 2D anisotropy function F(r,θ) (see Eq. (8) in TG-43U1) for r= 0.5 cm (c) and r = 4 cm (d), Kennedy et al. (Kennedy et al 2010) refer to TG-43U1 consensus MC data. Dolan et al. MC simulation and experimental data with LiF thermoluminscent dosimetry (TLD) are in reference (Dolan et al 2006).

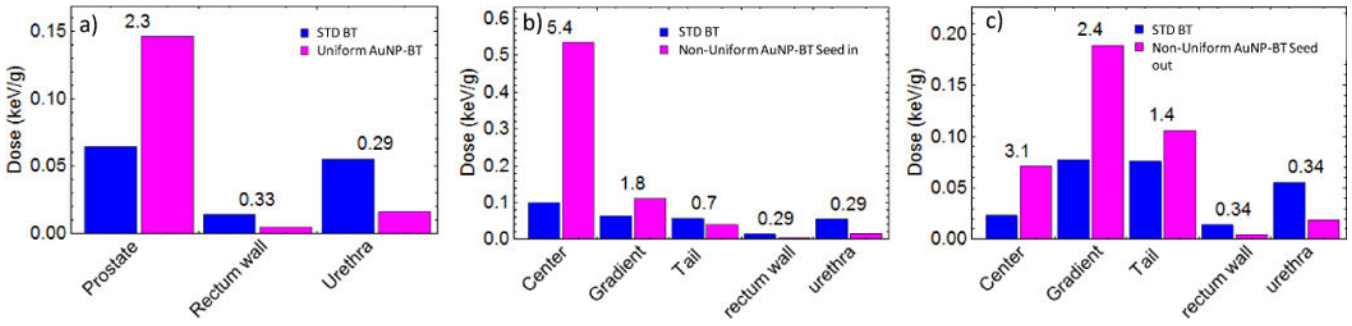

Figure 3.

Dose per incident x-ray in standard brachytherapy treatment (Blue) compared with the AuNP aided Brachytherapy treatment (Magenta) for a) uniform 30mg/g AuNP concentration, b) when brachytherapy needles (and so ^{125}I seeds) are centered in the region with high AuNP concentration (Center region), with c_{Center}=66mg/g, $c_{Gradient}$=33mg/g, c_{Tail}=10mg/g; c) when the ^{125}I seeds are in the Tail of the AuNP concentration, with c_{Center}=64.6mg/g, $c_{Gradient}$=32.3mg/g, c_{Tail}=10mg/g. Dose ratios between the two treatments are given on the top of the columns.

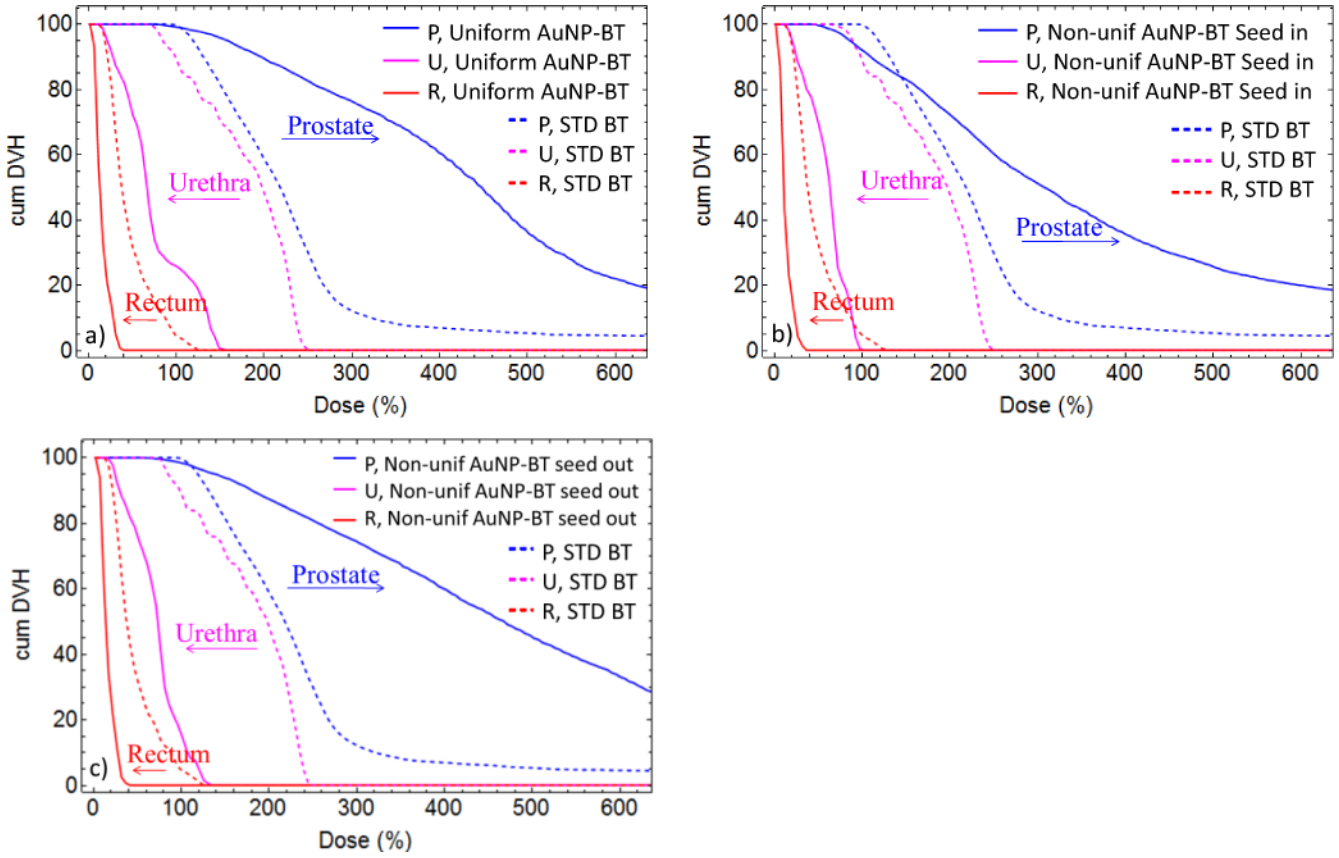

Figure 4.

Cumulative dose volume histogram over the life time of the ^{125}I seeds having air kerma strength of 1.467 U each. The prescribed minimal peripheral dose is 110Gy. Voxel dimensions are $0.2\times0.2\times0.2cm^3$ for the prostate (P) and rectum wall (R) and $0.1\times0.1\times0.2cm^3$ for the urethra (U). Dashed lines represent standard brachytherapy treatment while solid lines indicate the AuNP aided brachytherapy for a) uniform 30mg/g AuNP concentration, b) when the brachytherapy needles (and so ^{125}I seed) are centered in the region with high AuNP concentration (Center region), with c_{Center}=66mg/g, $c_{Gradient}$=33mg/g, c_{Tail}=10mg/g; c) when the ^{125}I seeds are in the Tail of the AuNP concentration, with c_{Center}=64.6mg/g, $c_{Gradient}$=32.3mg/g, c_{Tail}=10mg/g.

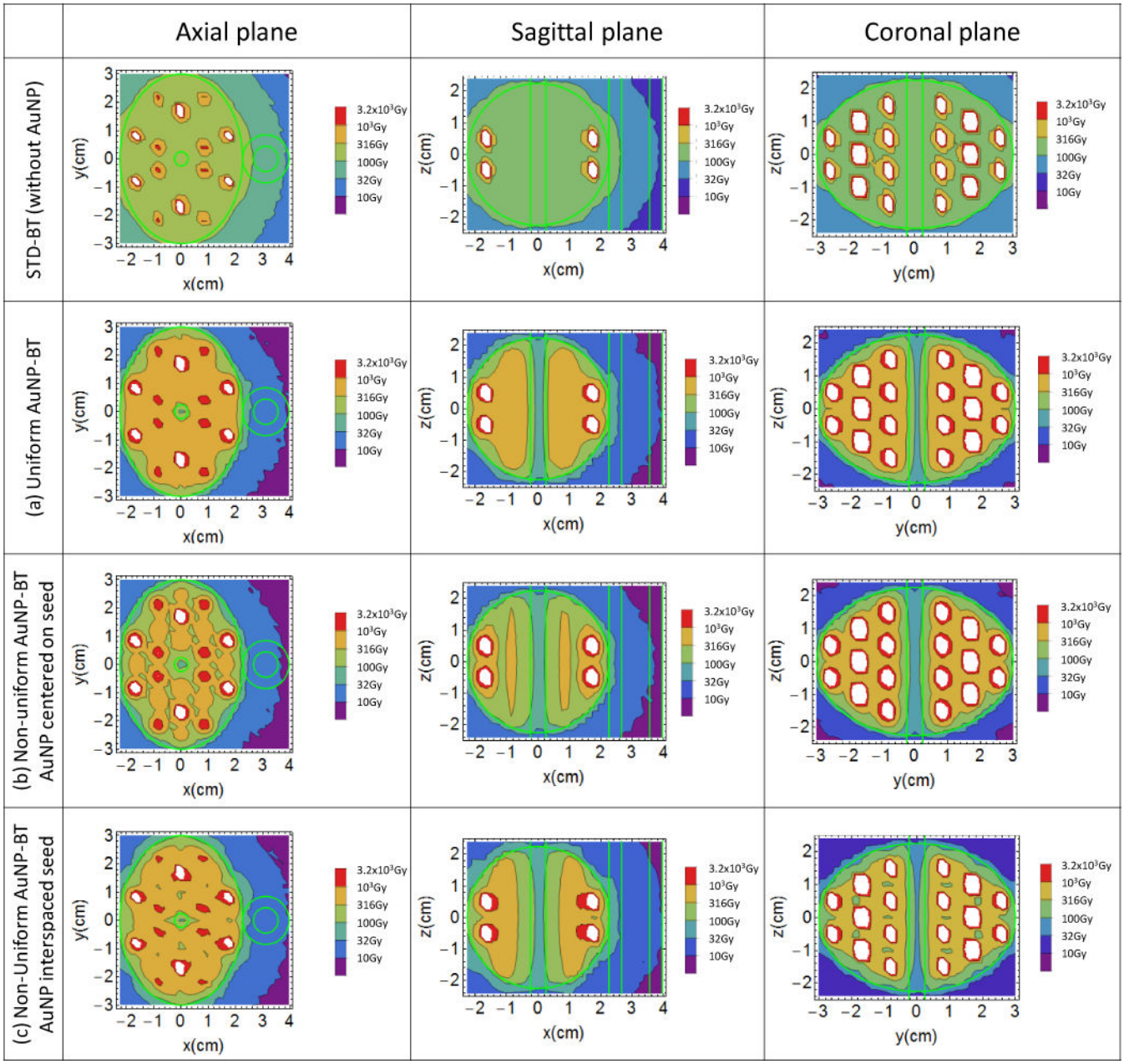

Figure 5.

dose distribution at the axial, sagittal and coronal planes at the center of the prostate for the STD-BT (first row) and a) uniform AuNP-BT, Non-Uniform AuNP-BT with AuNP centered on brachytherapy seeds (b) and interspaced between them (c).

Table 1

D90, V100, V150, V200, V250 and V300 for prostate and V100, D30, D10 for urethra and rectum under the different scenarios. mPD is the minimum peripheral dose set at 110Gy in the STD BT treatment. In parenthesis the ratio respect to the STD BT treatment.

	mPD=110Gy	STD BT	Uniform AuNP BT (case a)	Non-unif AuNP BT seed in (case b)	Non-unif AuNP BT seed out (case c)
Prostate	D90 (Gy)	144.0	216.6 (1.5×)	120.9 (0.84×)	198.1 (1.38×)
	V100 (%)	99.8	99.1 (0.99×)	92.1 (0.92×)	98.4 (0.986×)
	V150 (%)	81.6	95.8 (1.17×)	83.1 (1.02×)	93.8 (1.15×)
	V200 (%)	58.8	89.5 (1.52×)	72.3 (1.23×)	87.3 (1.48×)
	V250 (%)	30.0	82.6 (2.8×)	60.3 (2.01×)	80.9 (2.7×)
	V300 (%)	12.2	76.4 (6.3×)	51.2 (4.2×)	74.4 (6.1×)
Urethra	V100 (%)	89.6	25.9 (0.29×)	0.3 (0.003×)	15.7 (0.18×)
	D30 (Gy)	244.7	91.4 (0.37×)	77.6 (0.32×)	89.4 (0.37×)
	D10 (Gy)	259.3	150.3 (0.58×)	97.6 (0.38×)	118.5 (0.46×)
Rectum	V100 (%)	4.5	0	0	0
	D30 (Gy)	56.8	19.5 (0.34×)	16.3 (0.29×)	20.7 (0.36×)
	D10 (Gy)	74.3	31.2 (0.42×)	25.8 (0.35×)	30.4 (0.41×)